Linking Deprotonation and Denticity of Chelate Ligands. Rhenium(V) Oxo Analogues of Technetium-99m Radiopharmaceuticals Containing N_2S_2 Chelate Ligands

Luigi G. Marzilli,*,† Mariusz G. Banaszczyk,† Lory Hansen,† Zsuzsanna Kuklenyik,† Renzo Cini,‡ and Andrew Taylor, Jr.*,†

Departments of Chemistry and Radiology, Emory University, Atlanta, Georgia 30322, and Department of Chemistry, University of Siena, I-53100 Siena, Italy

Received July 14, 1994[⊗]

Carboxyl groups are important for efficient renal uptake of small anionic molecules. $[^{99m}TcO(ECH)]^{2-}$ (ECH = pentaanionic form of (2*R*,7*R*)-2,7-dicarboxy-3,6-diaza-1,8-octanedithiol (ECH_6)) is a potentially useful radiopharmaceutical for diagnosing renal function. As typically isolated, the $[^{99}Tc(V)O]^{3+}$ and $[Re(V)O]^{3+}$ derivatives of ECH_6 are neutral trifunctional acids, e.g., $^{99}TcO(ECH_3)$ and $ReO(ECH_3)$. The ligand has two carboxyl groups; the presence of the oxo group on the metal lowers the symmetry of the coordinated ligand, and one carboxyl group is *syn* and the other *anti* to the oxo group. Extremely broad NMR spectra at physiological pH and difficulty in crystallization have precluded complete characterization. Both the neutral species, $ReO(ECH_3)$ (**3**), and the ammonium salt of the trianionic species, $[NH_4]_3[ReO(EC)]\cdot C_4H_8O_2$ (**5**), have now been structurally characterized by X-ray diffraction. The coordination geometry of **3** is distorted octahedral, with the notable and unexpected feature that the *anti*-carboxylate group is coordinated trans to the oxo ligand. The coordination geometry of **5** is distorted square pyramidal, with the unusual feature that both nitrogen donor atoms are deprotonated. To determine the causes for the very broad ^1H and ^{13}C spectra of the Tc and Re complexes in aqueous solutions near physiological pH, we first prepared the analogous N_2S_2 ligand ($TMECH_6$) incorporating penicillamine (pen), which has no CH coupling. (The ECH_6 ligand is derived from cysteine (cys), which has a coupled three-spin system.) The acid dissociation constants of the Re EC and TMEC complexes were found to be similar, with one NH group partially deprotonated under physiological conditions. We then applied a battery of 2D NMR methods to Re derivatives of both N_2S_2 ligands in D_2O. From these studies, the EC ^1H NMR spin systems were identified and assigned for both acidic and basic aqueous solutions. From the Karplus relationship, the relevant torsion angles were calculated and compared to those determined crystallographically. These studies demonstrated that the *anti*-carboxyl group was coordinated in aqueous solution at low pH but not at high pH. The NMR results for $ReO(TMECH_3)$ under physiological conditions are consistent with *two* forms: (i) and *anti*-cys NH deprotonated, *anti*-carboxyl dissociated form and (ii) an *anti*-cys NH, coordinated *anti*-carboxyl form. The unusual broadening of $ReO(ECH_3)$ and $TcO(ECH_3)$ signals at pH 7 can be very confidently attributed to the coupling of carboxyl coordination and NH proton dissociation. Thus, proton dissociation makes the N a better donor. The resulting electronic and geometric changes at N favor deligation of the carboxyl group. On the NMR time scale, this process is in the intermediate exchange domain and leads to broad lines. The apparent pK_a near physiological pH is not a simple pK_a; the N_2S_2 ligand has different denticity in the acid and conjugate base forms of the complex. Molecular mechanics modeling suggests that *anti*-cys NH deprotonation leads to increased strain on the six-coordinate form, whereas *syn*-cys NH deprotonation has little effect. The most strain-free NH deprotonated quadridentate form has the *anti*-cys NH deprotonated. Thus, the calculations and the results of solution NMR and solid-state crystallography are all consistent.

Introduction

$^{99m}TcO(ECDH)$ ($ECDH_4$, (2*R*,7*R*)-2,7-dicarboxy-3,6-diaza-1,8-octanedithiol diethyl ester) (Chart 1) is a neutral lipophilic bis(amino thiol) (BAT) complex that crosses the blood brain barrier and is retained in the brain for several hours; the agent is currently being evaluated as a potential marker of regional cerebral blood flow.[1,2] Biodistribution studies have also shown that the renal extraction of the tracer from the systemic blood pool is very rapid. In vivo and in vitro studies have demonstrated that both the brain retention and renal excretion of $^{99m}TcO(ECDH)$ are a result of enzymatic de-esterification of the tracer to mono- and dicarboxylate metabolites.[3,4] These polar species are either trapped in the brain or eliminated from other body tissues by excretion into the urine. Of these metabolites, the dicarboxylate species, $[^{99m}TcO(ECH)]^{2-}$, is

Chart 1

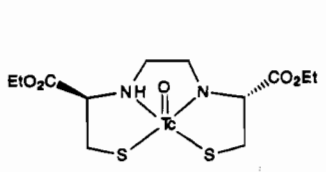

$^{99m}TcO(ECDH)$

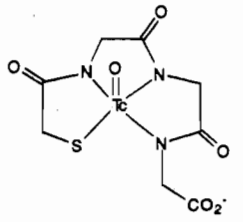

$[^{99m}TcO(MAG_3)]^{2-}$

† Emory University.
‡ University of Siena.
⊗ Abstract published in *Advance ACS Abstracts,* September 15, 1994.

(1) Walovitch, R. C.; Makuch, J.; Knapik, G.; Watson, A. D.; Williams, S. J. *J. Nucl. Med.* **1988**, *29*, 747.
(2) Verbruggen, A.; Bormans, G.; Van Nerom, C.; Cleyhens, B.; Crombez, D.; De Roo, M. In *Technetium and Rhenium in Chemistry and Nuclear Medicine 3*; Nicolini, M., Bandoli, G.; Mazzi, G., Eds.; Cortina International: Verona, Italy, 1990; p 445.

0020-1669/94/1333-4850$04.50/0

Chart 2

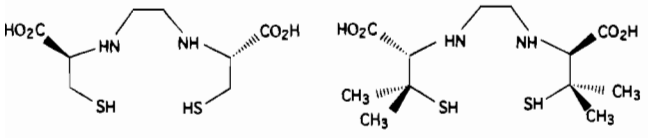

R,R-ECH$_6$ (1) S,S-TMECH$_6$ (2)

excreted into the urine most efficiently {ECH is the pentaanionic form of (2*R*,7*R*)-2,7-dicarboxy-3,6-diaza-1,8-octanedithiol (ECH$_6$)}.[5]

Rapid renal clearance of radiopharmaceuticals from the blood pool is generally desirable because it increases image quality (by lowering the background to target ratio) and also decreases the radiation dose to nontarget tissues.[6] The latter is particularly important in therapy of cancer with β-emitting radionuclides.[7] However, rapid renal clearance of a radiotracer is particularly useful in the evaluation of renal function.[8]

The efficient renal excretion of [^{99m}TcO(ECH)]$^{2-}$ prompted investigations into the potential usefulness of this agent as a renal function agent, and the results[5] have been promising in comparison to the clinically used renal agent, [^{99m}TcO(MAG$_3$)]$^{2-}$ (Chart 1). MAG$_3$ is the pentaanionic form of (mercaptoacetyl)-triglycine (MAG$_3$H$_5$). Biodistribution studies in mice showed that the renal excretion rate of [^{99m}TcO(ECH)]$^{2-}$ is comparable to that of [^{99m}TcO(MAG$_3$)]$^{2-}$ (94% vs 89% of the injected dose in the urine 30 min postinjection, respectively). Evaluation of [^{99m}TcO(ECH)]$^{2-}$ in rats and in human volunteers showed improvements[9] of some desired parameters of a renal function imaging agent over those of [^{99m}TcO(MAG$_3$)].$^{2-}$

As a part of our ongoing research in the development of new radiopharmaceuticals for imaging kidney function, we are currently exploring the chemistry of Re complexes with ECH$_6$ and related diamine dithiol (N_2S_2) ligand systems. This report concentrates on [Re(V)O]$^{3+}$ complexes prepared with ECH$_6$ (**1**) and (2*S*,7*S*)-2,7-dicarboxy-3,6-diaza-1,1,8,8-tetramethyl-1,8-octanedithiol (TMECH$_6$ (**2**)) (Chart 2). These ligands contain two *R*-cysteine (cys) or two *S*-penicillamine (pen) residues, respectively. The chemistry of Tc and Re complexes formed from ECH$_6$ is of particular interest because their characterization has been limited and they exhibit unusual properties at physiological pH (see below).[10] BAT complexes are also potentially

Chart 3

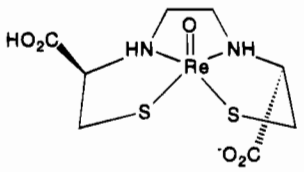

useful as ^{99m}Tc(V) brain imaging agents[1,2,11,12] and as ^{68}Ga(III) myocardial imaging agents for positron emission tomography.[13]

Re complexes are excellent structural models for Tc complexes because ^{99}Tc and Re complexes with identical ligands have essentially identical coordination parameters[14] and Re is an environmentally preferable, nonradioactive element. Additionally, although there are chemical shift differences between corresponding signals in the NMR spectra of [^{99}TcO(EC)]$^{3-}$ and [ReO(EC)]$^{3-}$ complexes in D_2O (with 3 equiv of NaOD), the spectra are similar and sharp.[10] At lower pH the spectra are broad and complicated for both the ^{99}Tc and Re analogues.[10] Complicated NMR spectra were also observed for a related ^{99}TcO(BAT) complex.[11a]

The neutral complexes MO(ECH$_3$) (M = ^{99}Tc, Re) have been prepared previously, and a square-pyramidal structure (Chart 3) was proposed by Edwards et al. on the basis of IR evidence.[10] Potentiometric titrations demonstrated that the neutral complexes are trifunctional acids. Dissociations of the second and third protons were attributed to amine deprotonation. Preliminary ^{1}H and ^{13}C NMR spectra of trianionic [MO(EC)]$^{3-}$ confirmed that both NHs are deprotonated. However, since the NMR spectra of species of intermediate protonation states, i.e. [MO(ECH$_2$)]$^-$ and [MO(ECH)]$^{2-}$, are indicative of fluxional or rapidly interconverting species, characterization of these species has been difficult. Furthermore, preliminary radiopharmaceutical formulation studies demonstrated that complexation of ECH$_6$ with ^{99m}Tc gives a good yield (>95%) at pH 12 but a poor yield (≈50%) at pH 7; the main impurity (unidentified) had a clinically unacceptable degree of hepatobiliary excretion.[5]

In order to understand better the complicated behavior of this system, the structures of the acidic and basic forms were determined by X-ray diffraction methods. The structure of ReO(ECH$_3$-3*NH*,4*NH*,6*O*) (**3**) has an unexpected 6-coordinate geometry, while [NH$_4$]$_3$[ReO(EC-3*N*,4*N*)]·C$_4$H$_8$O$_2$ (**5**) has a 5-coordinate geometry with both nitrogen donor atoms deprotonated. Ligands that can effectively delocalize negative charge such as dimercaptide−diamide ligands and *o*-aminobenzenethiol readily form [Tc^{V}O(N_2S_2)]$^-$ or [Re^{V}O(N_2S_2)]$^-$ species in which both nitrogen donor atoms are deprotonated.[11,15−17] To our knowledge, [NH$_4$]$_3$[ReO(EC-3*N*,4*N*)]·C$_4$H$_8$O$_2$ is the first reported [Tc(V)O]$^{3+}$ or [Re(V)O]$^{3+}$ N_2S_2 complex with both

(3) Vallabhajosula, S.; Zimmermann, M. P.; Picard, M.; Stritzke, P.; Mena, I.; Hellman, R. S.; Tikofsky, R. S.; Stabin, M. G.; Morgan, R. A.; Goldsmith, S. J. *J. Nucl. Med.* **1989**, *30*, 599.

(4) Walovitch, R. C.; Hill, T. C.; Garrity, S. T.; Cheesman, E. H.; Burgess, B. A.; O'Leary, D. A.; Watson, A. D.; Ganey, M. V.; Morgan, R. A.; Williams, S. J. *J. Nucl. Med.* **1989**, *30*, 1892.

(5) Verbruggen, A. M.; Nosco, D. L.; Van Nerom, C. G.; Bormans, G. M.; Adriaens, P. J.; De Roo, M. J. *J. Nucl. Med.* **1992**, *33*, 551.

(6) Axworthy, D. B.; Su, F-M.; Vanderheyden, J.-L.; Srinivasan, A.; Fitzner, J.; Galster, J.; Beaumier, P.; Fritzberg, A. R. *J. Nucl. Med.* **1991**, *32*, 915.

(7) (a) Griffiths, G. L.; Goldenberg, D. M.; Jones, A. L.; Hansen, H. J. *Bioconjugate Chem.* **1992**, *3*, 91. (b) Griffiths, G. L.; Goldenberg, D. M.; Knapp, F. F.; Callahan, A. P.; Chang, C.-H. *Cancer Res.* **1991**, *51*, 4594.

(8) Eshima, D.; Taylor, A., Jr. *Sem. Nucl. Med.* **1992**, *22*, 61.

(9) Banaszczyk, M. G.; Hansen, L.; Eshima, D.; Malveaux, G.; Taylor, A., Jr. Unpublished results. Jamar, F.; Stoffel, M.; Van Nerom, C.; Verbruggen, A.; Mourad, M.; Squifflet, J. P.; Beckers, C. *J. Nucl. Med.* **1993**, *34*, 129P (Abstract).

(10) Edwards, D. S.; Cheesman, E. H.; Watson, M. W.; Maheu, L. J.; Nguyen, S. A.; Dimitre, L.; Nason, T.; Watson, A. D.; Walovitch, R. In *Technetium and Rhenium in Chemistry and Nuclear Medicine 3*; Nicolini, M., Bandoli, G., Mazzi, U., Eds.; Cortina International: Verona, Italy, 1990; p 433.

(11) (a) Christy, S. J.; Francesconi, L. C.; Kung, H. F.; Wehrli, S.; Graczyk, G.; Carroll, P. *Polyhedron* **1992**, *10*, 1145. (b) Francesconi, L. C.; Graczyk, G.; Wehrli, S.; Shaikh, S. N.; McClinton, D.; Lui, S. *Inorg. Chem.* **1993**, *32*, 3114.

(12) Mahmood, A.; Baidoo, K. E.; Lever, S. Z. *Technetium and Rhenium in Chemistry and Nuclear Medicine 3*; Nicolini, M., Bandoli, G., Mazzi, U., Eds.; Cortina International: Verona, Italy, 1990; p 119.

(13) Francesconi, L. C.; Liu, B.-L.; Billings, J. J.; Carroll, P. J.; Graczyk, G.; Kung, H. F. *J. Chem. Soc., Chem. Commun.* **1991**, 94.

(14) Deutsch, E.; Libson, K. Vanderheyden, J.-L. *Technetium and Rhenium in Chemistry and Nuclear Medicine 3*; Nicolini, M., Bandoli, G., Mazzi, U., Eds.; Cortina International: Verona, Italy, 1990; p 13.

(15) Rao, T. N.; Adhikesavalu, D.; Camerman, A.; Fritzberg, A. R. *J. Am. Chem. Soc.* **1990**, *112*, 5798.

(16) Hansen, L.; Cini, R.; Taylor, A., Jr.; Marzilli, L. G. *Inorg. Chem.* **1992**, *31*, 2801.

(17) Bandoli, G.; Gerber, T. I. A. *Inorg. Chim. Acta* **1987**, *126*, 205.

nitrogens deprotonated in a ligand that cannot effectively delocalize the resulting lone pair. The structures of **3** and **5** are extremely important to the NMR characterization of the system.

Experimental Section

(*R*)-cysteine, (*S*)-penicillamine, NH_4ReO_4, THAM (tris(hydroxymethyl)aminomethane, ultra pure grade), and $SnCl_2{\cdot}H_2O$ were purchased from Aldrich and used as received. (4*S*)-5,5-dimethyl-1,3-thiazolidine-4-carboxylic acid,[18] $ReO_2I(PPh_3)_2$,[19] and $ReOCl_3(Me_2S)(OPPh_3)$[20] were prepared by literature methods.

Elemental analyses were performed by Atlantic Microlabs, Inc. The FTIR spectra were recorded with a Bruker IFS 66 instrument.

(2*R*,7*R*)-2,7-Dicarboxy-3,6-diaza-1,8-octanedithiol (ECH_6) (1). This compound was prepared analytically pure in 43% yield by the literature procedure.[21]

(2*S*,7*S*)-2,7-Dicarboxy-3,6-diaza-1,1,8,8-tetramethyl-1,8-octanedithiol Hemihydrate ($TMECH_6$) (2). This compound was prepared in 32% yield by the reductive coupling of (4*S*)-5,5-dimethyl-1,3-thiazolidine-4-carboxylic acid in liquid ammonia, an adaptation of the synthesis for ECH_6.[21] Anal. Calcd for $C_{12}H_{25}N_2O_{4.5}S_2$: C, 43.22; H, 7.56; N, 8.40; S, 19.23. Found: C, 42.91; H, 7.59; N, 8.34; S, 19.03. FTIR (cm^{-1}) in KBr: 1647, 1628, CO_2H; 1587, NH_2^+; 1382, CH_3-(sym); 1252, NH_2^+(twist).

Oxo(ECH_3-3*NH*,4*NH*,6*O*)rhenium(V) (ReO(ECH_3-3*NH*,4*NH*,6*O*) (3). A methanolic solution (50 mL) of $SnCl_2{\cdot}H_2O$ (4.51 g, 20 mmol, 50 mL) was added dropwise to an aqueous solution (50 mL) of ECH_6 (5.37 g, 20 mmol), $LiOH{\cdot}H_2O$ (12.59 g, 300 mmol), and NH_4ReO_4 (5.37 g, 20 mmol) under N_2. The mixture was heated at reflux overnight. After the mixture was cooled to 0 °C and filtered and the methanol removed *in vacuo*, the remaining aqueous orange solution was acidified to pH 2 with concentrated HCl. The purple microcrystalline needles (8.96 g, 96%) formed immediately were collected, rinsed with water, ethanol, and ethyl ether, and dried *in vacuo*. Anal. Calcd for $C_8H_{13}N_2O_5ReS_2$: C, 20.55; H, 2.80; N, 5.99; S, 13.71. Found: C, 20.36; H, 2.99; N, 5.89; S, 13.57. FTIR (cm^{-1}) in KBr: 1716, CO_2H; 1588, CO_2^-; 980, Re=O.

$ReO_2I(PPh_3)_2$ Method. A suspension of ECH_6 (537.7 mg, 2.0 mmol), $ReO_2I(PPh_3)_2$[19] (1.74 g, 2.0 mmol), and KOH (560 mg, 10 mmol) in a methanol−water mixture (40 mL, 50% v/v) was heated at reflux overnight, and the product was isolated as above in 99% yield.

$ReOCl_3(Me_2S)(OPPh_3)$ Method. A suspension of ECH_6 (268.3 mg, 1.0 mmol), $ReOCl_3(Me_2S)(OPPh_3)$[20] (650 mg, 1.0 mmol), and $LiOH{\cdot}H_2O$ (420 mg, 10 mmol) in methanol−water (20 mL, 50% v/v) was heated at reflux for ~1 h, giving the orange solution. After the solution was cooled at 0 °C, methanol was removed *in vacuo*. $OPPh_3$ was extracted with CH_2Cl_2 (3 × 25 mL), and the product was isolated as above in 75% yield.

Dicyclohexylammonium Oxo(ECH-3*NH*,4*N*)rhenium(V)−Ethanol ($[DCHA]_2$[ReO(ECH-3*NH*,4*N*)]·EtOH) (4). **3** (468 mg, 1 mmol) and dicyclohexylamine (363 mg, 2 mmol) were dissolved in refluxing methanol (20 mL). The resulting solution was cooled to 0 °C. The product was precipitated with Et_2O, collected, and dried *in vacuo*; yield, 712 mg (86%). An analytical sample was obtained by adding EtOH (1 mL) to a methanolic solution (1 mL) of the crude salt (100 mg). The resulting solution was placed in a small vial which was immersed in neat ethyl acetate. Crystals formed after a few days were collected and air dried. Anal. Calcd for $C_{34}H_{65}N_4O_6ReS_2$: C, 46.61; H, 7.48; N, 6.39; S, 7.32. Found: C, 46.61; H, 7.42; N, 6.13; S, 7.03. FTIR (cm^{-1}) in KBr: 1636, CO_2^-; 947, Re=O.

Ammonium Oxo(EC-3*N*,4*N*)rhenium(V)−1,4-Dioxane ($[NH_4]_3$-[ReO(EC-3*N*,4*N*)]·$C_4H_8O_2$) (5). An ammonia-saturated 1,4-dioxane solution (10 mL) was layered on top of a solution of **3** (234 mg, 0.5 mmol) in concentrated ammonium hydroxide (1 mL) in a screw cap vial. The crystals formed were quickly removed from the solution and dried in a stream of dried nitrogen. The crystal for the X-ray studies was removed from the solution just prior to the data collection. Anal. Calcd for $C_{12}H_{30}N_5O_7ReS_2$: C, 23.76; H, 4.98; N, 11.54; S, 10.57. Found: C, 23.84; H, 4.90; N, 11.61; S, 11.07. FTIR (cm^{-1}) in KBr: 1549 vs, CO_2^-; 872, Re=O.

Oxo($TMECH_3$-3*NH*,4*NH*,6*O*)rhenium(V) (ReO($TMECH_3$-3*NH*,-4*NH*,6*O*)) (6). $ReOCl_3(Me_2S)(OPPh_3)$ (389 mg, 0.6 mmol) and EtOH (20 mL) were added to an aqueous solution (10 mL) of **2** (167 mg, 0.5 mmol) and KOH (336 mg, 6.0 mmol) under nitrogen. The reaction mixture was heated at reflux for 3 h and then cooled to 0 °C. EtOH was evaporated *in vacuo*, and $OPPh_3$ was extracted with CH_2Cl_2 (3 × 10 mL). The pH was adjusted to 2.0 with concentrated HCl and the volume further reduced *in vacuo*, giving 204 mg (78%) of **6** as a reddish-brown powder. **6** can be recrystallized by dissolution in aqueous base followed by acidification to pH 2, but this procedure is not necessary to obtain analytically pure material. Anal. Calcd for $C_{12}H_{21}N_2O_5ReS_2$: C, 27.53; H, 4.04; N, 5.35; S, 12.25. Found: C, 27.51; H, 4.06; N, 5.26; S, 12.17. FTIR (cm^{-1}) in KBr: 1714 vs, 1612 vs, CO_2^-; 975 vs, Re=O.

X-ray Crystallography. The crystals of ReO(ECH_3-3*NH*,4*NH*,6*O*) (**3**) suitable for X-ray diffraction were grown by the slow diffusion of acetic acid vapors into a solution of **3** (268 mg, 0.5 mmol) and KOH (84 mg, 1.5 mmol) in H_2O (1 mL). The final pH of the mother liquor was 2.85. A purple crystal of **3** (0.38 × 0.20 × 0.18 mm) and a red crystal of **5** (0.30 × 0.28 × 0.20 mmol) were used for data collection. Intensity data for **3** were collected at room temperature. Crystals of **5** were extremely hygroscopic and unstable toward decomposition after being removed from the mother liquor. Therefore, data collection for **5** was performed at −100 °C by utilizing a LT2 low-temperature device. The crystal system and cell constants for **3** were determined by automatic indexing of 19 centered reflections. Final cell constants were calculated by least-squares refinement with 22 additional high-angle ($34° < 2\theta < 35°$) reflections. The crystal system and cell constants for **5** were determined from the automatic indexing of 15 centered reflections. Final cell constants were calculated by least-squares refinement with 15 additional high-angle ($24° < 2\theta < 25°$) reflections. Three check reflections were measured every 97 reflections for both crystals; there was no significant deviation in intensity. Lorentz and monochromator polarization corrections and semi-empirical absorption corrections based on azimuthal scans of selected reflections were applied. Both structures were solved by Patterson methods, and all non-hydrogen atoms were refined anisotropically by full-matrix least-squares procedures using SHELXTL PLUS (VMS). For **3**, the carboxyl H atom and one amine H atom (HN(2)) were located from difference maps. Since the Re−N(1) (2.151(18) Å) and Re−N(2) (2.153(18) Å) bond distances were similar and the second carboxylate appeared coordinated to Re, it was assumed that N(1) was also protonated, although a hydrogen atom could not be located from the difference map. The H atom (HN(1)) was generated at a calculated (d(N−H) = 0.96 Å) position. For **5**, the ammonium H atoms were located from difference maps and restrained using idealized N−H distances (0.95 Å) and H−N−H angles (109.5°). H atoms bound to carbon were generated at calculated (d(C−H) = 0.96 Å) positions for both structures. All H atoms were constrained using a riding model with isotropic thermal parameters fixed at 0.08. Crystal data and final refinement parameters are presented in Table 1.

1D ^1H and ^{13}C NMR Spectroscopy. 1D ^1H NMR spectra were recorded on GE 300, 500, or 600 or Nicolet 360 NMR spectrometers and referenced to internal TSP (3-(trimethylsilyl)propionic-2,2,3,3-d_4 acid, sodium salt). 1D ^{13}C NMR spectra, obtained on the GE 300 NMR spectrometer, were referenced to dioxane (69.12 ppm vs TSP). 2D spectra were acquired on GE 500 or 600 NMR spectrometers and processed with FELIX (Hare Research). Parameters are summarized in a supplementary table. All 2D spectra were referenced with the 1D ^1H and ^{13}C spectra.

Simulation of the 1D ^1H Spectra. The 1D ^1H NMR spectra were simulated with the GEMSIM program installed on the GE 500 NMR instrument. The signals were simulated separately for each spin system using the chemical shifts from the 1D ^1H NMR spectra. The coupling constants were changed systematically until the best fit between the experimental and calculated multiplet patterns was found.

(18) Sweetman, B. J.; Bellas, M.; Field, L. *J. Med. Chem.* **1969**, *12*, 888.
(19) Ciani, G. F.; D'Alfonso, G.; Romiti, P. F.; Sironi, A.; Freni, M. *Inorg. Chim. Acta* **1983**, *72*, 29.
(20) (a) Wilkinson, G.; Grove, D. E. *J. Chem. Soc. A* **1966**, 1224. (b) Bryan, J. C.; Stenkamp, R. E.; Tulip, T. H.; Mayer, J. M. *Inorg. Chem.* **1987**, *26*, 2283.
(21) Blondeau, P.; Berse, C.; Gravel, D. *Can. J. Chem.* **1967**, *45*, 49.

Table 1. Crystallographic Data for ReO(ECH$_3$-3*NH*,4*NH*,6*O*) (**3**) and [NH$_4$]$_3$[ReO(EC-^{3}*N*,4*N*)]·C$_4$H$_8$O$_2$ (**5**)

	3	**5**
chem formula	$C_8H_{13}N_2O_5ReS_2$	$C_{12}H_{30}N_5O_7ReS_2$
fw	467.53	606.73
space group	$P2_12_12_1$	$P2_12_12_1$
Z	4	4
a (Å)	6.298(1)	10.117(2)
b (Å)	10.061(2)	13.719(3)
c (Å)	19.669(4)	15.122(3)
V (Å^3)	1246.3(4)	2098.9(7)
d_{calcd} (g/cm^3)	2.49	1.92
μ (mm^{-1})	10.22	6.10
λ (Å)	0.710 73 (Mo Kα)	0.710 73 (Mo Kα)
T (K)	298	173
transm min/max (%)	1.02/2.70	1.77/3.62
R (%)	3.61	2.69
R_w (%)	4.77	3.70

pK_a Determinations. Potentiometric acid titrations were performed with 20 mM complex (5 mL) on a fully automated computerized titration system (SCHOTT GERATE TPC 2000; Great Lakes Chemicals) using 0.2 N HCl standardized against THAM. The pK_a values from at least three independent runs were calculated using the program associated with the system.

For the ^{1}H NMR titrations, a high pH stock solution in D_2O was prepared containing an internal standard [*tert*-butyl alcohol (1.25 ppm) or dioxane (3.76 ppm) vs TSP]. The pH (uncorrected) was adjusted with either NaOD or DCl. Spectra were promptly recorded, and the final pH was measured with a long stem pH electrode.

Molecular Mechanics. Calculations and graphics were performed with the MacroModel package (MMOD), version 3.0.[22] The force field used for the ligand part of each molecule was mostly AMBER[23] contained in MMOD, and the strain energy was computed as the sum of the bond length deformation (E_b), valence angle deformation (E_θ), torsion angle deformation (E_ϕ), nonbonding interaction (E_{nb}), and hydrogen-bonding interaction (E_{hb}) contributions: $E_{tot.} = E_b + E_\theta + E_\phi + E_{nb} + E_{hb}$. New force field parameters were developed in order to model coordination by the N(sp^3)(H) and the N(sp^3)(Lp) (Lp = lone pair) atoms to equatorial sites and by the *anti*-CO$_2^-$ to the distal site. Force field parameters not found in the original AMBER of MMOD or not previously reported in ref 16 were derived by a trial and error procedure in which the calculated structures of ReO(ECH$_3$-3*NH*,4*NH*,6*O*) and [ReO(EC-3*N*,4*N*,6*O*)]$^{3-}$ reached good agreement (supplementary material) with those observed via X-ray diffraction analysis of the crystals of **3** and **5**. All the other complexes were obtained by the construction procedure of MMOD, starting with the models of **3** and **5** as described.[16]

Results

Nomenclature. Ligands **1** and **2** have opposite chiralities, and the symmetry is lowered on coordination; one carboxylate group is *anti* and the other *syn* to the oxo ligand. Therefore, the basal coordination sites were numbered clockwise (EC) and counterclockwise (TEMC) in order to give the *anti* and *syn* halves the same numbers for complexes of both ligands (Chart 4).

1 and **2** have three types of dissociable protons (CO$_2$H, SH, NH) and are potentially hexaprotic acids. The state of protonation of the coordinated ligand must be indicated in designating the complex. Since the coordinated thiolate groups are always deprotonated, their protonation state is not specified. The *syn*-CO$_2$H is next most acidic in water; deprotonation is indicated by the number of Hs, e.g. ECH$_2$, and the overall charge of the complex. Coordination of the *anti*-CO$_2^-$ is specified as 6O; this group is not protonated in water. The two NHs can be both protonated (3NH,4NH) or deprotonated (3N,4N) or one of them protonated while the other one is deprotonated (3NH,-4N; 3N,4NH). For example, the neutral compound in Scheme 1 is named ^{99m}TcO(ECDH-3*NH*,4*N*) and the monoanionic EC complex with both amines protonated, the *syn*-CO$_2$H deprotonated, and the *anti*-CO$_2^-$ coordinated is designated as [ReO(ECH$_2$-3*NH*,4*NH*,6*O*)]$^-$. Protonation sites and *anti*-CO$_2^-$ coordination are not designated in uncertain cases.

Chart 4

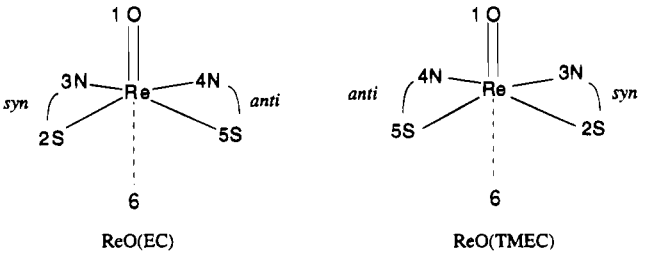

Table 2. Atomic Coordinates and Equivalent Isotropic Displacement Coefficients (Å^2 × 10^3) for ReO(ECH$_3$-3*NH*,4*NH*,6*O*) (**3**)

atom	x	y	z	U(eq)[a]
Re	9237(1)	1165(1)	1232(1)	34(1)
S(1)	6754(7)	1335(4)	384(2)	45(1)
S(2)	6953(7)	1475(5)	2140(2)	45(1)
N(1)	11066(22)	29(12)	512(6)	36(4)
N(2)	11147(22)	143(14)	1975(6)	41(4)
O(1)	10780(17)	2537(10)	1232(5)	51(3)
O(2)	10236(18)	−1432(11)	−1165(5)	49(3)
O(3)	13169(21)	−720(16)	−651(7)	73(5)
O(4)	8058(17)	−936(9)	1349(5)	40(3)
O(5)	7700(18)	−2569(11)	2090(5)	38(3)
C(1)	8283(25)	616(15)	−351(7)	36(5)
C(2)	9772(27)	−452(15)	−86(8)	39(5)
C(3)	11265(30)	−903(17)	−660(8)	46(6)
C(4)	12221(29)	−1074(16)	890(7)	43(5)
C(5)	12882(26)	−599(17)	1613(8)	45(5)
C(6)	9726(30)	−619(14)	2405(7)	39(5)
C(7)	8243(29)	331(16)	2739(7)	44(5)
C(8)	8417(26)	−1492(16)	1927(7)	37(5)

[a] Equivalent isotropic U defined as one-third of the trace of the orthogonalized U_{ij} tensor.

Synthetic Results. ReO(ECH$_3$-3*NH*,4*NH*,6*O*) (**3**) was prepared under basic conditions from ReOCl$_3$(Me$_2$S)(OPPh$_3$) and ReO$_2$I(PPh$_3$)$_2$, precursors used for the synthesis of N$_3$S (triamide−thiolate)[16] and triazacyclononane[24] complexes. [DCHA]$_2$[ReO(ECH-3*NH*,4*N*)]·EtOH (**4**) and [NH$_4$]$_3$[ReO(EC-3*N*,4*N*)]·C$_4$H$_8$O$_2$ (**5**) were prepared from **3**. **3** was also obtained by the direct reduction of ReO$_4^-$ in the presence of ECH$_6$ with SnCl$_2$ under basic (Experimental Section) or acidic (not described) conditions or with Na$_2$S$_2$O$_4$ under basic conditions. The one-step direct reduction procedure was the simplest method; however, the ReO$_2$I(PPh$_3$)$_2$ method gave better yields. Also, initial studies indicated that the sterically more demanding TMECH$_6$ would not form satisfactory amounts of ReO(TMECH$_3$) (**6**) on direct reduction of ReO$_4^-$. Analytically pure **6** was synthesized by the precursor method[16] from ReOCl$_3$(Me$_2$S)(OPPh$_3$).[20]

X-ray Structural Results. Final atomic coordinates for **3** and **5** are given in Tables 2 and 3, respectively. A perspective drawing of **3** is presented in Figure 1. The geometry is 6-coordinate with a carboxylate oxygen atom (O(4)) coordinated

(22) Still, W. C.; *et al.* MacroModel V3.0. Department of Chemistry, Columbia University, New York, NY.

(23) (a) Weiner, S. J.; Kollman, P. A.; Case, D. A.; Singh, U.; Ghio, C.; Alagona, G.; Profeta, S., Jr.; Weiner, P. *J. Am. Chem. Soc.* **1984**, *106*, 765. (b) Weiner, S. J. Kollman, P. A.; Nguyen, D. T.; Case, D. A. *J. Comput. Chem.* **1986**, *7*, 230.

(24) Conry, R. R.; Mayer, J. M. *Inorg. Chem.* **1990**, *29*, 4862.

Table 3. Atomic Coordinates ($\times 10^4$) and Equivalent Isotropic Displacement Coefficients ($Å^2 \times 10^3$) for $[NH_4]_3[ReO(EC\text{-}3N,4N)]\cdot C_4H_8O_2$ (**5**)

atom	*x*	*y*	*z*	*U*(eq)[a]
Re	9239(1)	503(1)	7740(1)	24(1)
S(1)	9418(3)	2190(2)	7888(2)	32(1)
S(2)	7589(3)	481(2)	8794(2)	35(1)
N(1)	9657(8)	821(6)	6490(5)	27(3)
N(2)	8089(8)	−420(6)	7158(5)	27(2)
O(1)	10591(7)	−98(5)	8191(4)	33(2)
O(2)	11965(7)	1119(5)	5505(5)	38(3)
O(3)	11088(8)	2436(5)	4907(5)	37(2)
O(4)	5584(7)	283(5)	6644(4)	33(2)
O(5)	4588(7)	−992(6)	7258(6)	46(3)
C(1)	10476(10)	2406(7)	6919(7)	31(3)
C(2)	9995(10)	1803(7)	6166(7)	29(3)
C(3)	11128(12)	1764(7)	5477(7)	30(4)
C(4)	8974(12)	263(7)	5803(7)	32(3)
C(5)	8367(11)	−645(8)	6215(7)	31(3)
C(6)	6897(10)	−848(7)	7517(6)	24(3)
C(7)	6886(11)	−722(8)	8531(7)	33(4)
C(8)	5591(11)	−481(8)	7099(7)	36(3)
C(9)	10023(20)	2716(14)	845(12)	85(5)
C(10)	9097(18)	2482(13)	146(11)	76(4)
O(6)	8329(10)	3370(7)	−48(7)	65(3)
C(11)	7725(25)	3822(17)	721(14)	118(7)
C(12)	8613(17)	3938(12)	1433(11)	71(4)
O(7)	9331(13)	3071(8)	1656(8)	83(3)
N(3)	7154(9)	−4464(7)	3391(6)	38(3)
N(4)	6340(9)	2272(6)	6922(6)	32(3)
N(5)	14599(9)	888(6)	4999(6)	28(3)

[a] Equivalent isotropic *U* defined as one-third of the trace of the orthogonalized U_{ij} tensor.

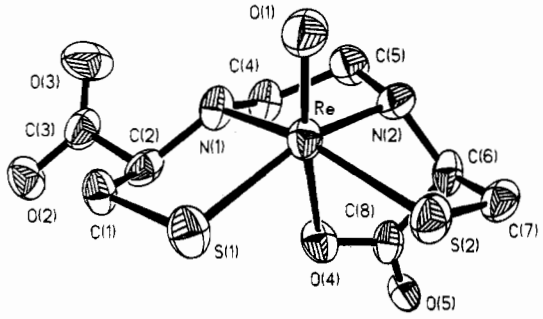

Figure 1. Perspective drawing of $ReO(ECH_3\text{-}3NH,4NH,6O)$ (**3**) with 50% probability for the thermal ellipsoids.

trans to the oxo ligand (O(1)) and Re displaced 0.45 Å from the ligand coordination plane toward the oxo ligand. Both the Re−N(1) (2.154(12) Å) and Re−N(2) (2.154(13) Å) bond distances (Table 4) are characteristic of bonding distances between Re(V) and neutral nitrogen donor atoms,[25] indicating that both N(1) and N(2) are protonated (leaving one carboxyl group deprotonated). Protonation (sp^3 hybridization) of N(1) and N(2) in **3** is also reflected in the Re−N(1)−C bond angles (113.1(10), 108.7(8)°) and Re−N(2)−C bond angles (108.8(9), 107.6(10)°). Both HN(1) and HN(2) are *syn* to the oxo ligand.

The Re−O(1) bond distance (1.688(10) Å) (Table 4) is within the range of distances (1.60(5)−1.73(6) Å) found in other Re(V)−oxo complexes.[15,16,26] However, the Re−O(4) bond distance (2.252(9) Å) is long even for a formal ReO single bond. Long bonds to atoms trans to multiply bonded oxo and nitrido ligands have been attributed to either steric repulsion of the *cis*-ligands[26,27] or to weak associations (of solvent molecules) to a

Table 4. Bond Distances (Å) and Bond Angles (deg) for $ReO(ECH_3\text{-}3NH,4NH,6O)$ (**3**) and $[NH_4]_3[ReO(EC\text{-}3N,4N)]\cdot C_4H_8O_2$ (**5**)

atoms	**3**	**5**
	Bond Distances (Å)	
Re−S(1)	2.293(4)	2.332(3)
Re−S(2)	2.314(4)	2.309(3)
Re−N(1)	2.154(12)	1.986(8)
Re−N(2)	2.154(13)	1.932(8)
Re−O(1)	1.688(10)	1.736(7)
Re−O(4)	2.252(9)	
	Bond Angles (deg)	
S(1)−Re−S(2)	97.3(1)	90.2(1)
S(1)−Re−N(1)	85.8(4)	81.8(2)
S(2)−Re−N(1)	155.7(3)	144.5(3)
S(1)−Re−N(2)	155.5(4)	137.8(3)
S(2)−Re−N(2)	83.6(4)	82.6(2)
N(1)−Re−N(2)	83.9(5)	80.7(3)
S(1)−Re−O(1)	109.4(4)	111.9(2)
S(2)−Re−O(1)	104.3(4)	107.0(2)
N(1)−Re−O(1)	97.3(5)	108.1(3)
N(2)−Re−O(1)	93.9(5)	110.0(3)
Re−S(1)−C(1)	100.4(5)	97.4(3)
Re−S(2)−C(7)	97.8(5)	98.1(4)
Re−N(1)−C(2)	113.1(10)	124.5(6)
Re−N(1)−C(4)	108.7(8)	117.4(6)
Re−N(2)−C(5)	108.8(9)	117.4(6)
Re−N(2)−C(6)	107.6(10)	126.6(6)
S(1)−Re−O(4)	85.4(3)	
S(2)−Re−O(4)	81.0(3)	
N(1)−Re−O(4)	75.2(4)	
N(2)−Re−O(4)	70.6(4)	
O(1)−Re−O(4)	163.2(4)	
Re−O(4)−C(8)	116.1(9)	

square-pyramidal unit.[28,29] The Re−O(4) bond distance in **3** is longer than the corresponding *trans*-Re−O distance (2.10(1) Å) in $ReOCl_2(acac)(PPh_3)$,[26] considered to be a distorted octahedron, and shorter than the *trans*-Re−O distance (2.32(4) Å) in *trans*-$[ReOBr_4(H_2O)]^-$ anion,[28] in which the H_2O molecule is considered to be only weakly coordinated to a square-pyramidal $[ReOBr_4]^-$ complex. However, the difference between the sum of the van der Waals radii (4.20 Å) of Re(V) (2.60 Å)[16] and O^- (1.60 Å)[23] and the Re−O(4) bond distance is 1.95 Å, and since the carboxylate group is not associated with a proton, coordination to the metal can be assumed. Furthermore, steric interaction between the coordinated carboxylate and the *cis*-ligands in **3** is a reasonable explanation for the long Re−O(4) bond in a formally octahedral coordination geometry in light of the small O(4)−Re−S and O(4)−Re−N bond angles (85.4(3)−70.6(4)°) (Table 4).

The Re−S(1) bond distance (2.293(4) Å) is within the range (2.282(2)−2.295(2) Å) observed in related Re(V) complexes with nitrogen−sulfur ligands.[15,16,30] The Re−S(2) bond distance (2.314(4) Å) is longer than the Re−S(1) bond distance, although not significantly.

A perspective drawing of **5** is presented in Figure 2. The coordination geometry of this species is clearly distorted square pyramidal; there are no intramolecular or intermolecular interactions between the carboxylate groups or oxygen atoms of the solvent molecule (dioxane) with the metal atom. The Re−N bond distances (1.986(8), 1.932(8) Å) are significantly shorter than those of $ReO(ECH_3\text{-}3NH,4NH,6O)$ (**3**) and are consistent with the bond distances observed in Re(V) complexes with

(25) Lock, C. J. L.; Turner, G. *Can. J. Chem.* **1977**, *55*, 333.
(26) Lock, C. J. L.; Wan, C. *Can. J. Chem.* **1975**, *53*, 1548.
(27) Bright, D.; Ibers, J. A. *Inorg. Chem.* **1969**, *8*, 709.
(28) Cotton, F. A.; Lippard, S. J. *Inorg. Chem.* **1965**, *4*, 1621.
(29) Cotton, F. A.; Lippard, S. J. *Inorg. Chem.* **1966**, *5*, 416.
(30) Rao, T. N.; Adhikesavalu, D.; Camerman, A.; Fritzberg, A. R. *Inorg. Chim. Acta* **1991**, *180*, 63.

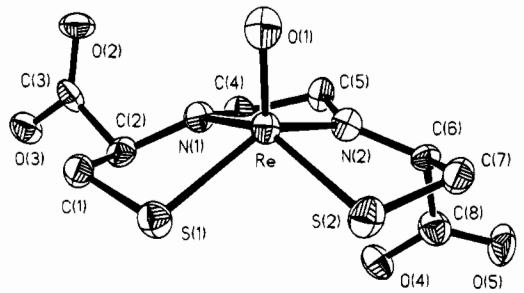

Figure 2. Perspective drawing of $[ReO(EC\text{-}3N,4N)]^{3-}$ (**5**) (trianion of **3**) with 50% probability for the thermal ellipsoids.

deprotonated nitrogen donor atoms (1.959(7)−2.04(2) Å).[15,16,30,31] The geometry about the nitrogen atoms in **5** is also reflective of deprotonation; the Re−N−C bond angles range from 117.4-(6) to 126.6(6)°. Furthermore, both Re−S bond distances (2.332(3), 2.309(3) Å) are comparable to those found in bis-(dithiolato)oxorhenium(V) complexes (2.309(8)−2.328(7) Å)[32,33] rather than those found in complexes with nitrogen−sulfur ligands.[15,16,30]

The Re atom is displaced 0.71 Å from the ligand coordination plane toward the oxo ligand. Although the Re−O(1) bond distance (1.736(7) Å) is longer than the corresponding distance in **3** (1.694(14) Å), it is within the range for a multiply bonded Re(V)−oxo group.[16,19,20] The N−Re−O bond angles are also significantly larger (~10°) in **5** than in **3** (Table 4). These parameters indicate that the coordination environment of Re is more tetragonally distorted in the complex's fully deprotonated form than in its fully protonated form; as a result, a five-coordinate geometry for $[ReO(EC\text{-}3N,4N)]^{3-}$ is favored.

H-bonding is extensive in the crystal lattice of **5**, involving all the oxygen atoms of the trianion and dioxane molecule with ammonium protons (supplementary material).

pH Dependence. We determined three pK_a's for **3** by potentiometric titrations in H_2O [pK_{a1} of 3.8 ± 0.5 (deprotonation of the *syn*-carboxyl group, difficult to determine because of precipitation); pK_{a2} of 6.64 ± 0.03, NH; pK_{a3} of 10.2 ± 0.2, NH]. The results are consistent with a report that **3** is a triprotic acid.[10] The apparent pK_{a2} was most reproducible, and the similar value for **6** (6.69 ± 0.04) suggests similar properties. Below, we show that "pK_{a2}" is not a simple pK_a.

NMR Spectroscopy of EC Complexes. As mentioned, the NMR spectral properties of the Tc and Re complexes of ECH_6 are very puzzling.[10] The ^{1}H NMR spectra have broad signals and are virtually uninterpretable near physiological pH. At low or high pH, sharp signals are observed but the spectra are not first order, even at high field.

Method of NMR Signal Assignment. In order to unravel this complexity, we carried out an extensive series of NMR experiments. These complexities required that we identify the spin systems (two cys residues and the ethylene bridge) and then simulate the ^{1}H NMR spectra to obtain coupling constants. Heteronuclear methods allowed us to relate the ^{1}H and the ^{13}C NMR signals, to distinguish which ethylene bridge ^{13}C NMR signal corresponds to the ethylene C closest to a particular cys residue, and to associate a carboxyl signal with that residue.

With the spin systems identified, we were faced with determining which signals were from the *syn*- and which were from the *anti*-half of the coordinated ligand. Since the overall

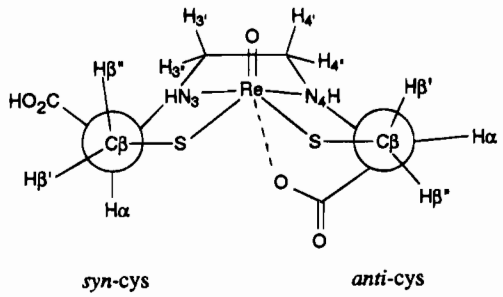

$ReO(ECH_3\text{-}3NH,4NH,6O)$

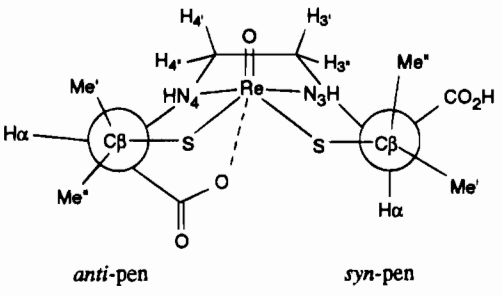

$ReO(TMECH_3\text{-}3NH,4NH,6O)$

Figure 3. Labeling scheme used for NMR assignments.

number of couplings should be similar, the final assignment rests on a comparison of coupling constants and relative intensity patterns of HMBC (heteronuclear multiple bond correlation) peaks to those expected from the X-ray torsion angles, which are different for the *syn*- and *anti*-residues. Assignment of the signals is described briefly in the Discussion section and in detail in the supplementary material.

The ^{1}H and ^{13}C labels used to discuss the NMR data are reported in Figure 3, and the ^{1}H and ^{13}C signal assignments are reported in Tables 5 and 6, respectively. The 1D ^{1}H, the HMBC, and the HMQC (heteronuclear multiple quantum correlation) NMR spectra of $[ReO(EC)]^{3-}$ at pH 13 are shown in Figure 4. We recorded the 1D ^{1}H NMR spectrum at pH 4.2 (Figure 5), where the peaks were sharp enough for comparison with the simulated spectra.

NMR Spectroscopy of TMEC Complexes. Method of NMR Signal Assignment. In the TMEC ligand the H_αs (Figure 3), which are not coupled in D_2O, give sharp singlets in acidic or basic conditions. We assigned the ^{1}H and ^{13}C signals to the pen residues and the ethylene on the basis of the $H_\alpha-C_\alpha$, $H_\alpha-CO_2^-$, $H_\alpha-C_\beta$, $H_\alpha-C_{Me}$, $H_\alpha-C_{3/4}$, $C_{3/4}-H_{4/3}$, and $C_\alpha-H_{Me}$ HMBC cross peaks. By acid titration we correlated the high pH with the low pH ^{1}H signals. At pH 7 two sets of signals were observed (these signals are broad but are distinguishable, unlike the EC complexes). The H_α signals from the same pen residues of the two forms were correlated by saturation transfer. The assignment to *anti*- and *syn*-pen residues is described briefly in the Discussion section.

Informative HMBC Cross Peak Patterns. For $[ReO(TMEC)]^{3-}$ at pH 13, both H_α signals gave stronger and weaker HMBC peaks with the $C_{Me'}$ and $C_{Me''}$ signals (Figure 6). However, the weaker peak is much weaker for the downfield H_α (assigned to the *anti*-pen) than for the upfield H_α (assigned to the *syn*-pen). The strong $H_\alpha-C_{Me}$ HMBC cross peak from the *anti*-H_α signal at pH 13 became a weak peak at pH 3 (Figure 6), while the relative intensities of the signals from the *syn*-H_α were about the same at both pHs.

Molecular Mechanics Calculations. The results of the

(31) Danopoulos, A. A.; Wong, A. C. C.; Wilkinson, G.; Hursthouse, M. B.; Hussain, B. *J. Chem. Soc., Dalton Trans.* **1990**, 315.
(32) Blower, P. J.; Dilworth, J. R.; Hutchinson, J. P.; Nicholson, T.; Zubieta, J. *J. Chem. Soc., Dalton Trans.* **1986**, 1339.
(33) Clegg, W.; Boyde, S.; Garner, C. D. *Acta Crystallogr.* **1988**, *C44*, 172.

Table 5. ^{1}H NMR Chemical Shifts (ppm) and Assignments for Rhenium(V) Oxo Complexes

compd, solvent, pH	*syn*-cys			*anti*-cys			ethylene bridge	
	H_α	$H_{\beta'}/H_{Me'}$	$H_{\beta''}/H_{Me''}$	H_α	$H_{\beta'}/H_{Me'}$	$H_{\beta''}/H_{Me''}$	$H_{3'}$, $H_{3''}$	$H_{4'}$, $H_{4''}$
[ReO(EC-3*N*,4*N*)]$^{3-}$, D_2O, 13.0	3.59	3.61	2.84	4.42	3.19	3.39	4.04, 3.26	3.98, 3.76
[ReO(ECH_2-3*NH*,4*NH*,6*O*)]$^-$, D_2O, 4.2	4.47	3.11	3.62	4.41	4.09	3.32	3.65,[a] 2.86[a]	3.98,[a] 3.81[a]
[ReO(TMEC-3*N*,4*N*)]$^{3-}$, D_2O, 13.0	3.55	1.82	1.34	4.11	1.52	1.67	3.95, 3.02	3.95, 3.52
[ReO($TMECH_2$-3*NH*,4*NH*,6*O*)]$^-$, D_2O, 3.0	3.29	2.05	1.51	4.07	1.94	1.64	3.60, 2.84	4.01, 3.67

[a] Tenative assignment on the basis of (a) assigning the most upfield signal from the ethylene bridge to $H_{3''}$ and (b) 1D ^{1}H coupling data.

Table 6. ^{13}C NMR Chemical Shifts (ppm) and Assignments for Rhenium(V) Oxo Complexes

compd, solvent, pH	*syn*-cis					*anti*-cys					ethylene bridge	
	C_α	C_β	$C_{Me'}$	$C_{Me''}$	CO_2	C_α	C_β	$C_{Me'}$	$C_{Me''}$	CO_2	C_3	C_4
[ReO(EC-3*N*,4*N*)]$^{3-}$, D_2O, 13.0	88.90	47.95			186.66	84.03	48.15			185.06	69.38	67.90
[ReO(TMEC-3*N*,4*N*]$^{3-}$, D_2O, 13.0	95.78	60.52	32.57	30.18	183.96	93.89	59.91	36.51	29.74	183.96	68.70	67.77
[ReO(TMEC-3*NH*,4*NH*,6*O*)]$^-$, D_2O, 3.0	80.52	73.80	31.88	27.32	175.55	82.49	66.28	31.69	30.19	179.88	58.16	59.29

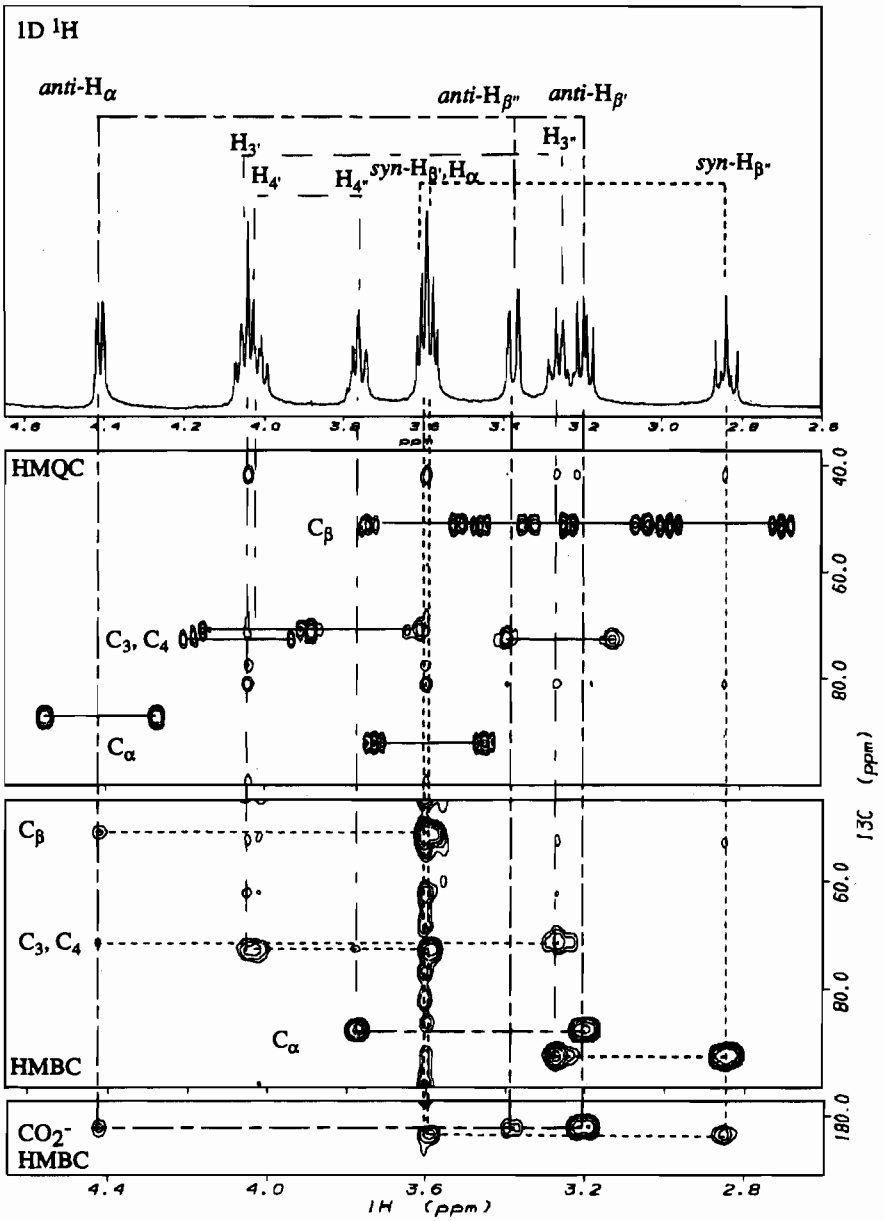

Figure 4. 1D ^{1}H, HMQC, and HMBC NMR spectra of [ReO(EC-3*N*,4*N*)]$^{3-}$ in D_2O at pH 13.

molecular mechanics calculations performed with MMOD on ReO(ECH_3-3*NH*,4*NH*,6*O*) (**3**) and [ReO(EC-3*N*,4*N*)]$^{3-}$ (**5**) are presented in the supplementary material. All the calculated and found bond distances and bond angles agree well for both **3** and **5**. The superimposition rms values, based on the coordination sphere atoms, were 0.082 and 0.089 Å, respectively. The new force field parameters are given in Table 7. The strain energy calculations will be discussed below.

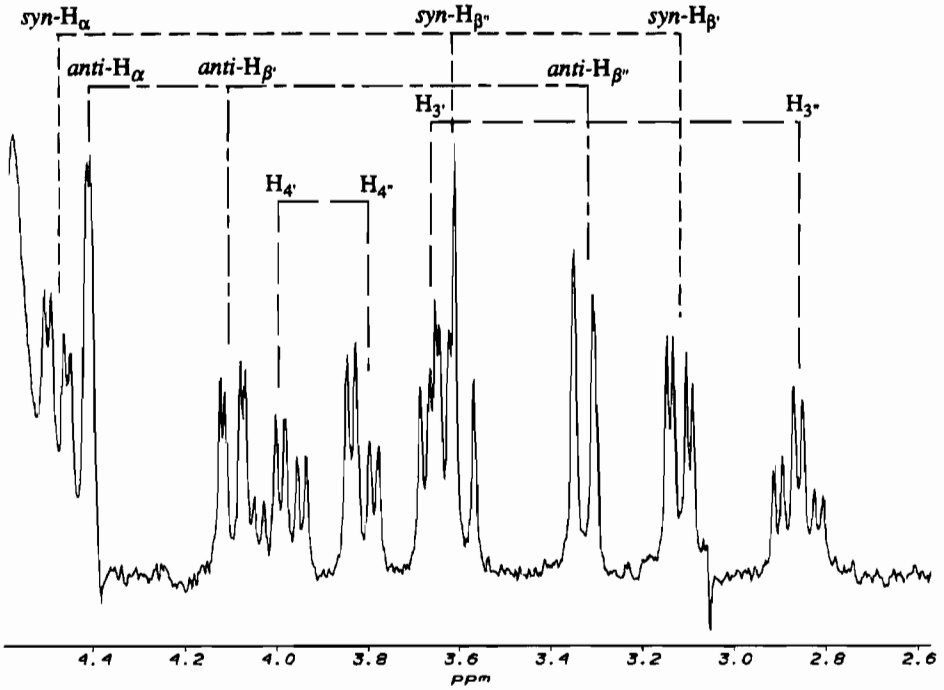

Figure 5. 1D ^{1}H NMR spectrum of [ReO(ECH$_2$-3*NH*,4*NH*,6*O*)]$^-$ at pH 4.2.

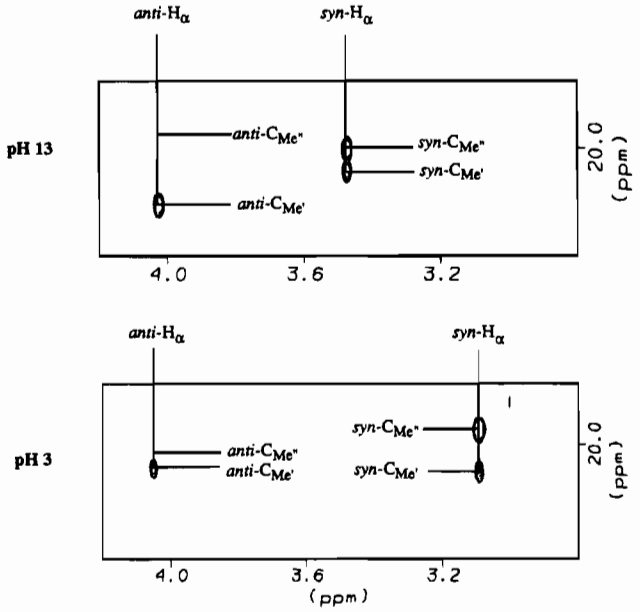

Figure 6. Partial HMBC NMR spectra of [ReO(TMEC-3*N*,4*N*)]$^{3-}$ (pH 13) and [ReO(TMECH$_2$-3*NH*,4*NH*,6*O*)]$^-$ (pH 3) in D_2O.

Discussion

This study was undertaken because the nature of the [^{99m}TcO(ECH)]$^{2-}$ complex that is rapidly excreted in the urine was unclear; therefore, the properties of this species that facilitate rapid renal transport were unclear. The X-ray structures of the triacid (**3**) and of the trianion (**5**) provide the first reported detailed information on the system. The complexes represent the two practical extremes in protonation state[34] (Figure 7) and delineate the effect of these extremes on structure.

Various possible states of protonation and N_2S_2 ligand denticity are outlined in Figure 7. In the figure, we do not show the possibility that H_2O is coordinated in the sixth position when the *anti*-CO_2^- group is not coordinated. The NMR data do not allow us to distinguish between Re(V)=O and H_2O—Re(V)=O axial ligation nor between a rapid equilibrium between these forms.

(34) ReO(ECH$_3$) is insoluble in trifluoroacetic acid and 1 N HCl.

Table 7. Force Field Parameters Not Included or Different from Those Found in the AMBER File of MMOD or in Ref 16[a]

bond	R_0, Å	K,[b] (kcal·Å^{-2})/mol
Re=O	1.70	400.0
Re−N(sp^3)(H)	2.15	100.0
Re−N(sp^3)(Lp)	1.99	130.0
Re−O	2.24	100.0
N(sp^3)(Lp)−C(sp^3)	1.45	355.0
N(sp^3)(H)−C(sp^3)	1.50	300.0
N(sp^3)−Lp	0.55	600.0
N(sp^3)−H	1.05	553.0
angle	θ_0, **deg**	K[c], (kcal·rad^{-2})/mol
S−Re−O	85.0	15.0
S−Re−N(sp^3)(Lp)	84.0	49.0
S−Re−N(sp^3)(H)	84.0	49.0
S−Re−N(sp^3)(Lp)-*trans*	140.0	49.0
S−Re−N(sp^3)(H)-*trans*	156.0	49.0
O=Re−O	180.0	15.0
O=Re−N(sp^3)(Lp)	109.0	49.0
O=Re−N(sp^3)(H)	95.0	49.0
O−Re−N(sp^3)(Lp)	74.0	15.0
O−Re−N(sp^3)(H)	74.0	15.0
N(sp^3)−Re−N(sp^3)	84.0	49.0
Re−O−H	109.0	35.0
torsional terms	$V1$, **kcal/mol**	$V2$, **kcal/mol**	$V3$, **kcal/mol**
Re−S−C(sp^3)−C(sp^3)	0.0	0.9	0.1
Re−N(sp^3)−C(sp^3)−C(sp^3)	0.0	0.4	0.4
Re−N(sp^3)−C(sp^3)−C(sp^2)	0.0	−0.3	0.15
Re−O−C(sp^2)−C(sp^3)	0.0	1.0	0.0
Re−O−C(sp^2)−O	0.0	1.0	0.0

[a] Amber substructure (atom type from MMOD): ZO(=O2)−S1−C3−C3−N3(*1)−C3−C3−N3(*1)−C3−C3−S1(−1). [b] $E_b = \sum_{bonds} K(R - R_o)^2$. [c] $E_\theta = \sum_{angles} K(\theta - \theta_o)^2$.

Structures of ReO(ECH$_3$-3*NH*,4*NH*,6*O*) (3) and [ReO(EC-3*N*,4*N*)]$^{3-}$ (5). There is a dramatic structural change from **3**, a distorted octahedron, to **5**, a distorted square pyramid. The

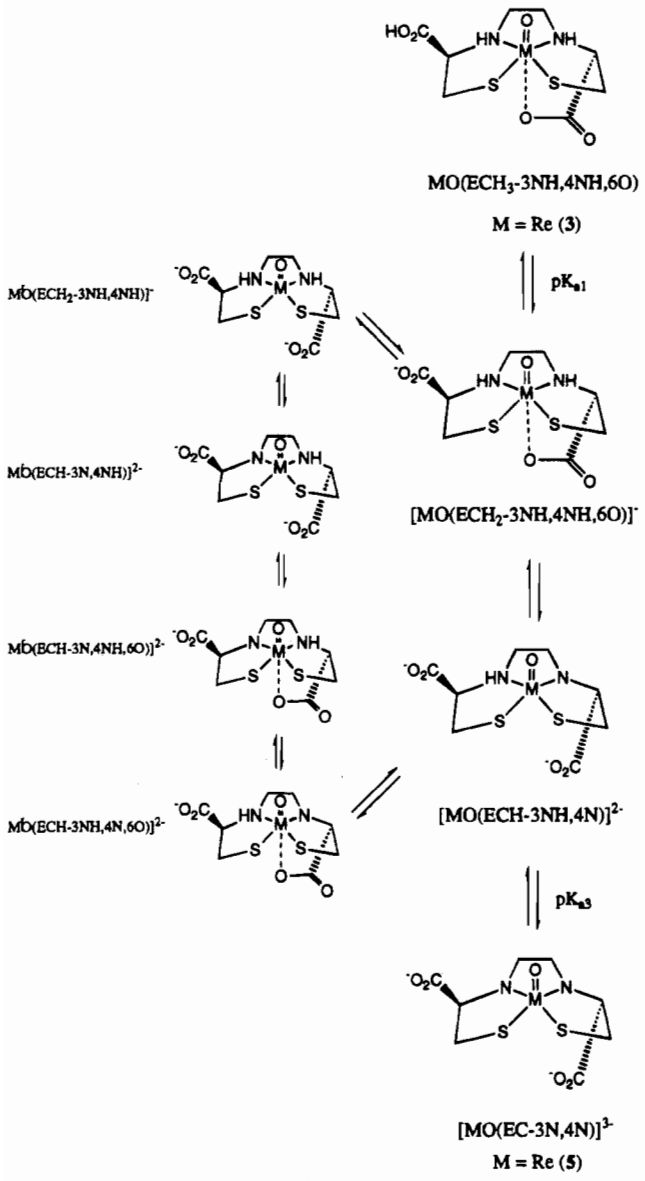

Figure 7. Possible equilibria for complexes (M = ^{99}Tc, Re) derived from the ECH_6 ligand. Analogous equilibria are possible for complexes derived from the $TMECH_6$ ligand.

Re=O stretching frequency[35] is shifted from 980 cm^{-1} in ReO(ECH_3-3*NH*,4*NH*,6*O*) to 872 cm^{-1} in $[ReO(EC\text{-}3N,4N)]^{3-}$. An intermediate value was found for **4** (947 cm^{-1}). The deprotonated N's are excellent donors and weaken the Re=O bond. This change in electronic properties contributes to the structural change. The solid-state structures and electronic properties of ReO(ECH_3-3*NH*,4*NH*,6*O*) and $[ReO(EC\text{-}3N,4N)]^{3-}$ bracket those of the species present at physiological pH and provide models for accurately and quantitatively interpreting NMR spectroscopic data.

Structures of $[ReO(ECH_2\text{-}3NH,4NH,6O)]^-$ and $[ReO(EC\text{-}3N,4N)]^{3-}$ in D_2O. As mentioned above, the NMR signal assignment to *syn*- and *anti*-cys residues required comparison of the coupling constants determined by NMR spectroscopy to those expected from torsion angles in the X-ray structures (Table 8).

Calculation of Torsion Angles and Assignment Strategy. Normally torsion angles are derived from coupling constants through a Karplus type equation:[36] $^3J = 11.0\cos^2\Phi - 1.4\cos\Phi + 1.6\sin^2\Phi$. Although the calculation of torsion angles with the Karplus equation is sometimes problematic due to the presence of electronegative atoms as well as substantial angular strain,[37] the equation used was developed for the thiazolidine ring.[36] Fortunately, the *syn*- and the *anti*-cys residues are in two rather different conformations and, therefore, the equation is accurate enough for our purposes, namely, to (i) calculate ^3J from solid-state data, (ii) evaluate the similarities between the solution-state and solid-state structures, and (iii) monitor the conformational changes as a function of pH (Table 8).

Table 8. Comparison of Coupling Constants and Torsion Angles for ReO(EC) Complexes

cys	$^3J_{\alpha\beta'}$,[a] Hz	$H_\alpha C_\alpha C_\beta H_{\beta'}$,[b] deg	$^3J_{\alpha\beta''}$,[a] Hz	$H_\alpha C_\alpha C_\beta H_{\beta''}$,[b] deg
		pH 4.2 $[ReO(ECH_2\text{-}3NH,4NH,6O)]^-$		
syn	4.0 (4.4)	−54 (−51) [−52]	12.8 (12.1)	−180[c] (−170) [−171]
anti	3.0 (4.2)	62 (53) [54]	<3.0[d] (2.7)	<−62[d] (−65) [−65]
		pH 13.0 $[ReO(EC\text{-}3N,4N)]^{3-}$		
syn	5.4 (5.6)	−44 (−43) [−47]	12.7 (11.4)	−180[c] (−162) [−168]
anti	8.0 (6.9)	26 (34) [39]	2.3 (1.6)	−69 (−86) [−81]

[a] Observed (calculated, solid-state) value. Coupling constants calculated from eq $^3J = 11.0\cos^2\Phi - 1.4\cos\Phi + 1.6\sin^2\Phi$ using a torsion angle Φ obtained from X-ray structures. [b] Torsion angles from NMR data, from X-ray data in parentheses, and from molecular mechanics calculations in brackets. NMR torsion angles were calculated with the above quadratic equation using the observed coupling constants. [c] $^3J > 12.4$ Hz (the ^3J maxima of the equation at $\Phi = \pm 180°$). [d] Only signal broadening was observed, consistent with a $^3J < 3$ Hz. The torsion angle could not be calculated but should be $<-62°$.

The relative intensity of the HMBC cross peaks can be used to estimate qualitatively the $^1H-^{13}C$ coupling constants because the peak intensity is linearly related to the coupling constant.[38] The HMBC coupling pattern supports the conclusions about torsion angles predicted by the $^1H-^1H$ coupling constants.

In the *syn*-cys residue (Figure 3) the $H_\alpha-C_\alpha-C_\beta-H_{\beta'}$ torsion angle is *gauche*, the $H_\alpha-C_\alpha-C_\beta-H_{\beta''}$ torsion angle is *trans*, and both the $H_{\beta'}-C_\beta-C_\alpha-CO_2^-$ and the $H_{\beta''}-C_\beta-C_\alpha-CO_2^-$ torsion angles are *gauche*. In the *anti*-cys residue both the $H_\alpha-C_\alpha-C_\beta-H_{\beta'}$ and the $H_\alpha-C_\alpha-C_\beta-H_{\beta''}$ torsion angles are *gauche*, the $H_{\beta'}-C_\beta-C_\alpha-CO_2^-$ torsion angle is *trans*, and the $H_{\beta''}-C_\beta-C_\alpha-CO_2^-$ torsion angle is *gauche*. Therefore the conformation of the *syn*- and *anti*-cys residues could be clearly distinguishable by NMR spectroscopy. The *syn*-cys residue signals were assigned from small $H_\alpha-H_{\beta'}$ and large $H_\alpha-H_{\beta''}$ vicinal coupling constants in the 1D ^1H spectrum and from weak $H_{\beta'}-CO_2^-$ and $H_{\beta''}-CO_2^-$ cross peaks in the HMBC spectrum. At the same time *anti*-cys signals were assigned from the small $H_\alpha-H_{\beta'}$ and $H_\alpha-H_{\beta''}$ coupling constants in the 1D ^1H spectrum and from a strong $H_{\beta'}-CO_2^-$ and a weak $H_{\beta''}-CO_2^-$ HMBC cross peak. Details are provided in the supplementary material.

Torsion Angles at High pH. The torsion angles, $H_\alpha-C_\alpha-C_\beta-H_{\beta'}$ and $H_\alpha-C_\alpha-C_\beta-H_{\beta''}$, calculated from the coupling constants (Table 8) agree reasonably well with those found in the crystal structure, e.g. −44° vs −43° and ca. −180° vs −162° and e.g. 26° vs 34° and −69° vs −86°, from the *syn*-cys and *anti*-cys residues (Figure 3), respectively.

If the cys residue assignments were interchanged, the conformation of the *anti*- and *syn*-cys residues in solution would be opposite to those in the solid. The *anti*-CO_2^- group would be directed away from the center of the coordination sphere (Chart 5). However, the *syn*-CO_2^- would be very close to the oxo ligand, an unlikely situation.

(35) (a) Barraclough, C. G.; Lewis, J.; Nyholm, R. S. *J. Chem. Soc. A* **1959**, 3552. (b) Nugent, W. A.; Mayer, J. M. *Metal Ligand Multiple Bonds*; Wiley & Sons: New York, 1988; p 112.

(36) Kopple, K. D.; Wiley, G. R.; Tauke, R. *Biopolymers* **1973**, *12*, 627.
(37) Karplus, M. *J. Am. Chem. Soc.* **1963**, *85*, 2870.
(38) Bax, A.; Summers, M. F. *J. Am. Chem. Soc.* **1986**, *108*, 2093.

Chart 5

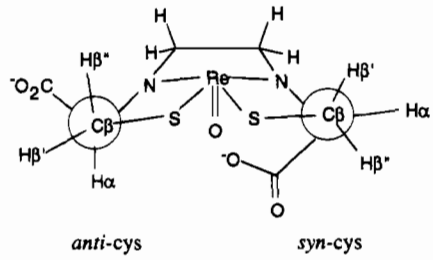

Torsion Angles at Low pH. The $H_\alpha-C_\alpha-C_\beta-H_{\beta'}$ and $H_\alpha-C_\alpha-C_\beta-H_{\beta''}$ torsion angles calculated from the coupling constants are −54 and ca. −180° for the *syn*-cys, and 62 and <−62° for the *anti*-cys, respectively. These torsion angles agree well with those in the solid state: −51 and −170° for the *syn*-cys and 53 and −65° for *anti*-cys, respectively.

Comparison of Conformations at High and Low pH. From pH 13 to 4.2, the two cys residues exhibit small but interesting changes in conformation. For the *anti*-cys, the $H_\alpha-C_\alpha-C_\beta-H_{\beta'}$ torsion angle decreases from 62 to 26°. The change in the $H_\alpha-C_\alpha-C_\beta-H_{\beta''}$ torsion angle could not be determined accurately in D_2O since at low pH the $^3J_{\alpha\beta''}$ values are less than the line width. However, in the solid the torsion angle increases (−65 to −86°). This 36° (NMR) or 21° (solid-state) rotation around $C_\alpha-C_\beta$ bond of the *anti*-cys residue suggests that at high pH the *anti*-CO_2^- is positioned farther from the negatively charged $[ReO(N_2S_2)]^-$ coordination sphere than at low pH. On decrease of the pH, the torsion angles $H_\alpha-C_\alpha-C_\beta-H_{\beta'}$ and $H_\alpha-C_\alpha-C_\beta-H_{\beta''}$ for the *syn*-cys residue increase by only 9° (NMR) and 8° (solid), respectively. Thus, the *syn*-cys residue undergoes a smaller conformational change than the *anti*-cys residue. In the ethylene bridge, $^3J_{3''4'}$ increased and $^3J_{3'4''}$ decreased (supplementary material), indicating that the $N_3-C_3-C_4-N_4$ torsion angle increases from pH 13 to 4.2. This change is consistent with the X-ray results: 28° in **5**, 44° in **3**.

Assignments for [ReO(TMECH$_2$-3*NH*,4*NH*,6*O*)]$^-$ and [ReO(TMEC-3*N*,4*N*)]$^{3-}$. On the basis of the ReO(EC) complexes, the *syn*-pen residue of both $[ReO(TMEC)]^{3-}$ and $[ReO(TMECH_2)]^-$ should have *trans* $H_\alpha-C_\alpha-C_\beta-C_{Me''}$ and *gauche* $H_\alpha-C_\alpha-C_\beta-C_{Me'}$ torsion angles, which are pH insensitive. Therefore, from the *syn*-pen residue a strong $H_\alpha-C_{Me''}$ and a weak or medium $H_\alpha-C_{Me'}$ HMBC cross peak are expected regardless of pH. The $H_\alpha-C_\alpha-C_\beta-C_{Me''}$ and $H_\alpha-C_\alpha-C_\beta-C_{Me'}$ torsion angles of the *anti*-pen residue should both be *gauche* and change with pH. Therefore, for the *anti*-pen residue we expect medium $H_\alpha-C_{Me'}$ and weak $H_\alpha-C_{Me''}$ HMBC peaks at high pH but weak HMBC peaks at low pH. The observed HMBC cross peak patterns are very similar to those expected (Figure 6). The upfield H_α signals have strong and weak HMBC peaks at both low and high pH; thus, these were assigned to the *syn*-pen residues. The downfield H_α signals gave strong and very weak HMBC cross peaks at high pH and weak and very weak cross peaks at low pH; these were thus assigned to the *anti*-pen residues (Tables 5 and 6). As for $[ReO(EC)]^{3-}$, the stereospecific assignment of the ethylene signals were based on the strong *syn*-C_α-H3″ and *anti*-C_α-H4″ HMBC cross peaks.

Physiological Form(s). The NMR data (Figure 8) clearly show that there are two forms present simultaneously near physiological pH. The two species need to be identified. The questions are as follows for each form present: (i) Which NH is deprotonated? (ii) Is the *anti*-CO_2^- coordinated? (iii) What is the coordination number? The factors leading to the rather broad pH 7 spectra also need to be identified. The analysis of these questions can be divided into two parts. First, we assess

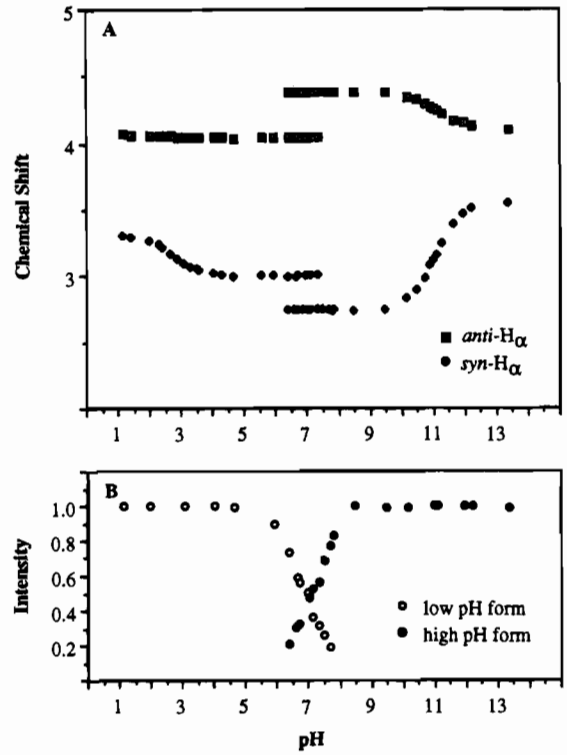

Figure 8. Dependence of ^{1}H NMR spectrum of [ReO(TMEC-3*N*,4*N*)]$^{3-}$ on the addition of acid.

Table 9. Strain Energy Values for the Minimized Structures

structure	$E_{tot.}$, kcal/mol
ReO(ECH$_3$-3*NH*,4*NH*,6*O*)	20.5[a] (*syn*-3NH, *syn*-4NH)
	23.9 (*anti*-3NH, *syn*-4NH)
	55.3 (*syn*-3NH, *anti*-4NH)
	52.3 (*anti*-3NH, *anti*-4NH)
ReO(ECH$_3$-3*NH*,4*NH*)	19.0
[ReO(ECH-3*NH*,4*N*)]$^{2-}$	20.8
[ReO(ECH-3*NH*,4*N*)(H$_2$O)]$^{2-}$	27.8
[ReO(ECH-3*NH*,4*N*,6*O*)]$^{2-}$	29.4
[ReO(ECH-3*N*,4*NH*)]$^{2-}$	22.3
[ReO(ECH-3*N*,4*NH*)(H$_2$O)]$^{2-}$	31.4
[ReO(ECH-3*N*,4*NH*,6O)]$^{2-}$	23.4
[ReO(EC-3*N*,4*N*)]$^{3-}$	24.0[b]
	23.6
[ReO(EC-3*N*,4*N*,6*O*)]$^{3-}$	31.6

[a] Similar to the crystal structure. [b] Two minima were found. The two structures have a different orientation of the *anti*-CO_2^- plane with respect to the $C(sp^2)(CO_2)$ axis (N−C−C−O, −11.7 and −102.4°, respectively).

the structural features using molecular mechanics calculations. Next, we consider the experimental data.

From the calculated strain energies ($E_{tot.}$, Table 9) of the minimized structures, it must be noted that [ReO(ECH-3*NH*,4*N*)]$^{2-}$ is more stable (~2 kcal/mol) than [ReO(ECH-3*N*,4*NH*)]$^{2-}$. The main destabilizing contribution for [ReO(ECH-3*N*,4*NH*)]$^{2-}$ comes from the repulsive nonbonding interactions between $C(sp^2)$ (*anti*-CO_2^-) (*anti*-CO_2^-) and the metal atom. This contact causes tension in the bond angles around the $4N(sp^3)$ donor. The calculations clearly show that deprotonation of the *anti*-cys NH, 4NH, is favored for the monodeprotonated quadridentate ligand not only in the five-coordinate forms but also in the six-coordinate forms axially ligated by water.

The strain energy of [ReO(ECH-3*NH*,4*N*,6*O*)]$^{2-}$ is higher by about 6 kcal/mol than that of [ReO(ECH-3*N*,4*NH*,6*O*)]$^{2-}$ owing to the high E_θ contribution from the bond angles around the $4N(sp^3)$ donor atom when the *anti*-CO_2^- group is coordinated.

The difference in the strain energies of ReO(ECH$_3$-3*NH*,4*NH*,6*O*) and ReO(ECH$_3$-3*NH*,4*NH*) (~1.5 kcal/mol) is much lower than the difference in the strain energies of [ReO(EC-3*N*,4*N*,6*O*)]$^{3-}$ and [ReO(EC-3*N*,4*N*)]$^{3-}$ (~8 kcal/mol). These comparisons show that the protonation of the *anti*-cys N atom (4N) facilitates the coordination of *anti*-CO_2^- by positioning one oxygen atom near coordination position 6.[39]

TcO(ECDH-3*NH*,4*N*) (Scheme 1) isolated at pH 7.0 was demonstrated crystallographically to have 4N deprotonated.[10] In DMSO-d_6, we found clear evidence for 4NH deprotonation to produce a carboxyl group deligated form.[40] In the acid titration of [ReO(TMEC-3*N*,4*N*)]$^{3-}$, the *syn*-pen H_α signal broadens and shifts to a greater degree from pH 13 to 10 (Figure 8) than the *anti*-pen signal, which is still sharp. Thus, 4N is deprotonated by pH 10, and pK_{a3} is assigned to 3NH (*syn*-pen or *syn*-cys NH) deprotonation. The calculations, the NMR data in D_2O (and DMSO)[40] for ReO(TMEC), and the solid-state structure of TcO(ECDH-3*NH*,4*N*) are all consistent with 4NH deprotonation near physiological pH and 3NH deprotonation near pH 10.

The monoprotonated 3NH species formed at ~pH 10 in the acid titration of [ReO(TMEC-3*N*,4*N*)]$^{3-}$ was present from pH 10 to ~6. The chemical shifts of the *anti*-H_α and the *syn*-H_α signals of this species do not change below pH 10 (Figure 8). However, below pH 8 both H_α signals present at high pH became broad and *decreased* in intensity, and a *second* set of broad signals emerged. Between pH 8 and 6, the two forms were present. The signals of the second form *increased* in intensity and clearly became those of the six-coordinate ReO(TMECH$_3$) on further lowering of the pH. The second form must have a second proton added, and this adds to N4 giving [ReO(TMECH$_2$-3*NH*,4*NH*,6*O*)]$^-$. As expected, as the pH was lowered further, the *syn*-H_α signal shifted on protonation of the uncoordinated *syn*-CO_2^-. This process is fast on the NMR time scale.

These spectral changes and our 2D NMR results establish that the second (low pH) form has a coordinated *anti*-CO_2^- and coordination starts to occur near physiological pH. Forms that exist above pH 8 all have quadridentate CO_2^- deligated N_2S_2 ligand. The intersection of the peak intensity−pH curves from the CO_2^--coordinated (low pH) and CO_2^--uncoordinated (high pH) forms was at pH 6.9 ± 0.2 (Figure 8), near the potentiometrically determined "pK_{a2}", 6.69, in H_2O. The absence of shift changes for the signals of the pH 10 form on lowering the pH demonstrates that the quadridentate N_2S_2 ligand in [ReO(TMECH-3*NH*,4*N*)]$^{2-}$ does *not* become protonated without a change in ligation. At pH ~6.5, protonation of the N_2S_2 ligand leads to a complex with a quinquedentate ligand, [ReO(TMECH$_2$-3*NH*,4*NH*,6*O*)]$^-$. These findings agree with the calculations.

Under physiological conditions, there are significant amounts of only two species, [ReO(TMECH-3*NH*,4*N*)]$^{2-}$ and [ReO(TMECH$_2$-3*NH*,4*NH*,6*O*)]$^-$, because coordination of the *anti*-CO_2^- and protonation of the 4N are coupled. The broadness of the signals indicates that the rate of equilibration between these two species is in the intermediate time domain on the NMR time scale. This protonation−deprotonation linked change in N_2S_2 ligand ligation is supported by the calculations and must also occur for the Tc and Re EC complexes. However, for EC complexes, the $^1H-^1H$ coupling combined with exchange broadening precludes an interpretation of the NMR spectra near the neutral pH range. Only *four* of the eight possible species in Figure 7 exist to any significant extent. These four are shown enlarged on the right in Figure 7.

There is still the question of the coordination number of [ReO(TMECH-3*NH*,4*N*)]$^{2-}$. This species could have water bound as an axial ligand. The experiments do not rule out this possibility since our methods do not provide direct evidence on this point; in general, determination of the involvement of solvent in metal coordination is difficult. We are confident that the very high pH dideprotonated form is five coordinate since the monodeprotonated species, ReO(ECDH-3*NH*,4*N*), is five coordinate in the solid state. Dideprotonation should greatly favor the five-coordinate form. As stated above, the conclusions drawn from the calculations for the two [ReO(TMECH)(H_2O)]$^{2-}$ species axially ligated by water (Table 9) are unaffected in terms of the preferential deprotonation site being 4NH. All of our NMR data and the underlying causes of the broadening at physiological pH can be explained equally well for either coordination form of [ReO(TMECH-3*NH*,4*N*)]$^{2-}$.

Summary and Implications. The broadness observed in the NMR spectrum of the TcO(EC) radiopharmaceutical at physiological pH is a consequence of the presence of two forms in intermediate exchange on the NMR time scale. These forms differ principally in the denticity of the N_2S_2 ligand. The proton dissociation is thus not a simple process, and there is no simple pK_a. A similar process may explain the complicated behavior of other Tc radiopharmaceuticals. Conceivably, only one of the two forms of TcO(EC) may be transported efficiently by the kidneys, and identification of this form could lead to the design of an agent with exclusively the characteristics which optimize transport.

These findings have implications *beyond* the field of radiopharmaceutical chemistry. Deligation at one end of a chelate due to deprotonation at a remote site may be widespread in coordination chemistry but may go undetected because changes in (e.g., UV−vis, IR, etc.) spectra occur on deprotonation even in the absence of deligation.

Acknowledgment. We thank David Hamilton and Prof. Harry P. Hopkins for assistance with the acid titrations and use of instrumentation and acknowledge financial support from the National Institutes of Health (Grant No. DK38842-04).

Supplementary Material Available: Crystallographic data [tables of calculated (MMOD) and observed (X-ray) geometrical parameters, crystallographic data, anisotropic displacement coefficients, and H-atom coordinates with isotropic displacement coefficients and stereoviews of the X-ray structures for **3** and **5**; a table of H-bonding contacts for **5**] and NMR data [a table and text giving 2D NMR parameters and NMR assignments and figures showing simulation of the 1D ^1H spectra] (17 pages). Ordering information is given on any current masthead page.

(39) In the solid-state structure of ReO(ECH$_3$-3*NH*,4*NH*,6*O*) (**3**) and the calculated structures of ReO(ECH$_3$-3*NH*,4*NH*,6*O*) and ReO(ECH$_3$-3*NH*,4*NH*) both NH protons are *syn* with respect to the oxo group. Calculated structures of ReO(ECH$_3$-3*NH*,4*NH*,6*O*) with *anti*-3NH, *anti*-4NH protons ($E_{tot.}$ = 52.3 kcal/mol) and *syn*-3NH, *anti*-4NH protons ($E_{tot.}$ = 55.3 kcal/mol) are relatively high in strain energy (Table 9). An *anti*-4NH proton decreases the Re−4NH bond length to 2.03 Å (ideal = 2.15 Å) and the bond angles around the 4N atom deviate from ideal values (110°) up to 20°. Consequently, the E_b and E_θ contributions to $E_{tot.}$ are high. The bond lengths and angles involving the 3N atom show much smaller distortions when the 3NH proton is *anti* (vs *syn*). $E_{tot.}$ of ReO(ECH$_3$-3*NH*,4*NH*,6*O*) with the *anti*-3NH, *syn*-4NH protons (23.9 kcal/mol) is only 3.4 kcal/mol higher than that of ReO(ECH$_3$-3*NH*,4*NH*,6*O*) with both NH protons *syn*. However, the geometry of the $-CH(CO_2H)-CH_2-$ group in the *anti*-3NH, *syn*-4NH complex shows significant deviations from that in the solid-state or calculated structures of **3**.

(40) Marzilli, L. G.; Hansen, L.; Kuklenyik, Z.; Cini, R.; Banaszczyk, M. G.; Taylor, A., Jr. Manuscript in preparation.